# OUTSTANDING MEETING PAPERS

*Papers in this section are based on submissions to the MRS Symposium Proceedings that were selected by Symposium Organizers as the outstanding paper. Upon selection, authors are invited to submit their research results to* Journal of Materials Research*. These papers are subject to the same peer review and editorial standards as all other JMR papers. This is another way by which the Materials Research Society recognizes high quality papers presented at its meetings.*

## Nanosphere lithography fabricated plasmonic materials and their applications

Xiaoyu Zhang,[a] Chanda Ranjit Yonzon,[a] and Richard P. Van Duyne[b]
*Department of Chemistry, Northwestern University, Evanston, Illinois 60208-3113*

(Received 4 November 2005; accepted 23 January 2006)

Nanosphere lithography fabricated nanostructures have highly tunable localized surface plasmons, which have been used for important sensing and spectroscopy applications. In this work, the authors focus on biological applications and technologies that utilize two types of related plasmonic phenomena: localized surface plasmon resonance (LSPR) spectroscopy and surface-enhanced Raman spectroscopy (SERS). Two applications of these plasmonic materials are presented: (i) the development of an ultrasensitive nanoscale optical biosensor based on LSPR wavelength-shift spectroscopy and (ii) the SERS detection of an anthrax biomarker.

### I. INTRODUCTION

The last two decades have seen a tremendous advancement of noble metal nanostructures as optical chemosensing and biosensing platforms in environmental protection,[1,2] medical diagnostics,[3–5] drug screening,[6] food safety,[2,7] and homeland security.[8] The optical properties, especially the plasmonic properties, of noble metal nanostructures are used in the development of a new class of optical biosensors. On the most elementary level, surface plasmons exist in two simple forms: propagating plasmons and localized surface plasmons. Propagating surface plasmons are evanescent electromagnetic waves bounded by flat, smooth metal-dielectric interfaces and arise from oscillations of the conduction electrons in the metal.[9] When surface plasmons are confined on periodic,[10] colloidal,[11] or other nanosystems,[8] localized optical modes are observed. Localized surface plasmon resonance (LSPR) results in wavelength-selective absorptions with extremely large molar extinction coefficients ($\sim 10^{11}$ $m^{-1}$ $cm^{-1}$),[12] resonant Rayleigh scattering with efficiency equivalent to that of $10^6$ fluorophores,[13] and enhanced local electromagnetic fields near the surface of the nanoparticle that are responsible for the intense signals observed in surface-enhanced Raman spectroscopy (SERS).[14] Strong electromagnetic fields are generated when the LSPR of nanoscale roughness features on a silver, gold, or copper substrate is excited by light.[15,16] When the Raman scatterer is subjected to these intensified electromagnetic fields, the magnitude of the induced dipole increases, and accordingly, the intensity of the inelastic scattering increases.[14] This phenomenon is known as surface-enhanced Raman scattering and can be exploited for sensitive and selective molecular identification.

It is well established that the peak wavelength of the LSPR spectrum is dependent upon the geometry of the nanoparticle as well as its own dielectric properties and those of its local environment including the substrate, solvent, and adsorbates.[17] In this work, nanosphere lithography was used to fabricate silver nanoparticle arrays with highly tunable plasmons (Fig. 1). The tunability of noble nanostructures has been exploited to act as a signal transduction mechanism for molecular sensing. This review captures two important optical sensors utilizing the nanosphere lithography (NSL) fabricated nanostructures, and therefore, it will be organized into two parts. First, we will demonstrate a LSPR sensor for a carbohydrate binding protein and compare the sensing performance of the nanoparticle-based LSPR sensor with the flat surface plasmon resonance (SPR) sensor. Second, we will highlight a SERS sensor for calcium dipicolinate, an anthrax biomarker.

[a]These authors contributed equally to this work.
[b]Address all correspondence to this author.
e-mail: vanduyne@chem.northwestern.edu
This paper was selected as the Outstanding Meeting Paper for the 2005 MRS Spring Meeting Symposium R Proceedings, Vol. 876E.
DOI: 10.1557/JMR.2006.0136

  

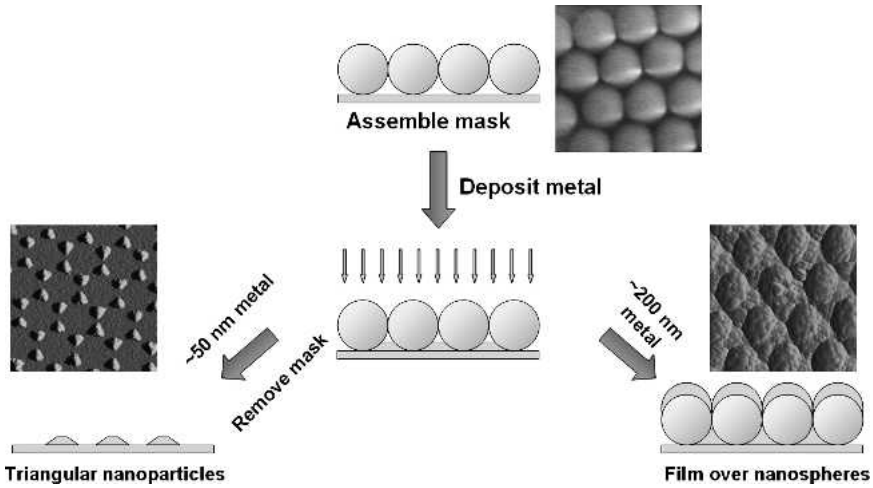


FIG. 1. Schematic illustration of the nanosphere lithographic fabrication of nanoparticle arrays (left side) and film over nanosphere surfaces (FON; right side) and corresponding micrographs.

## II. EXPERIMENTAL

### A. Materials

Ag (99.99%) was purchased from D.F. Goldsmith (Evanston, IL) and Au (99.99%) was acquired from Materials Research (Orangeburg, NY). Tungsten vapor deposition boats were purchased from R.D. Mathis (Long Beach, CA). Glass substrates were 18-mm-diameter, No. 2 coverslips from Fisher Scientific (Fairlawn, NJ). Pretreatment of glass substrates required $H_2SO_4$, $H_2O_2$, and $NH_4OH$, which were obtained from Fisher Scientific. Surfactant-free, white carboxyl-substituted polystyrene latex nanospheres with diameters of 390 nm from Duke Scientific (Palo Alto, CA) and 600 nm from Interfacial Dynamics (Portland, OR) were received as suspensions in water. Ti was purchased from Aldrich (Milwaukee, WI). Phosphate buffered saline (PBS), pH = 7.4 was obtained from Sigma (St. Louis, MO). Absolute ethanol was purchased from Pharmco (Brookfield, CT). For all steps of substrate preparation, water purified with cartridges from Millipore (Marlborough, MA) to a resistivity of 18 MΩ cm was used. Nitric acid 70% (Fisher Scientific), dipicolinic acid (2,6-pyridinedicarboxlic acid, DPA), calcium hydroxide, and benzenethiol (Aldrich) were used as purchased.

### B. Synthesis

The compounds 11-mercaptoundecyl tri(ethyelene glycol) disulfide (EG3), malemide terminated disulfide, mannose thiol, and galactose thiol were synthesized as described in the literature.[18] Calcium dipicolinate was prepared from DPA and calcium hydroxide according to the method of Beiley and co-workers.[19]

### C. Nanosphere lithography

NSL is a powerful fabrication technique that inexpensively produces nanoparticle arrays with controlled shape, size and interparticle spacing. Glass substrates were pretreated in two steps (i) piranha etch, 1:3 30% $H_2O_2$:$H_2SO_4$ at 80 °C for half an hour to clean the substrate, and (ii) base treatment, 5:1:1 $H_2O$:$NH_4OH$:30% $H_2O_2$ with sonication for 1 h, which rendered the surface hydrophilic. Both piranha etch and base treatment were done in the hood with appropriate safety goggles and lab coats. The pretreated glass was coated by solution casting using approximately 2 μl undiluted nanosphere solution (10% wt/wt%). The nanospheres were allowed to dry in ambient conditions to form a two-dimensional (2D) hexagonally close packed array. Ag was thermally deposited on the sphere mask. The Ag nanoparticles were obtained by sonicating the substrate in absolute ethanol for 3 min for LSPR sensing whereas the spheres were left intact resulting into Ag film over nanospheres (AgFON) for SERS sensing.

### D. SPR and LSPR sensor preparation

For the SPR sensor, Au (50 nm) was evaporated on glass coverslips with a thin Ti underlayer (10 nm) for adhesion of Au. For the LSPR sensors, NSL created Ag nanoparticle arrays were used. The self-assembled monolayer (SAM) was prepared by immersing the coverslips in an ethanolic solution containing 450 μl tri(ethylene glycol) disulfide (EG3), (1 mM), and 50 μl maleimide-terminated disulfide, (1 mM). After 12 h, the coverslips were rinsed with ethanol and dried under a stream of nitrogen. The substrates presenting maleimide-functional groups were immersed in methanolic solutions of 5 mM mannose thiol, for 40 min The mannose thiol covalently binds to malemide, providing ~5% sugar-immobilized surfaces, based on the fraction of starting thiols and efficiency of the malemide reaction. The mannose-functionalized sensors were then exposed to Concanavalin A for 20 min.

### E. SPR spectroscopy

A BIACore 1000 (Neuchâtel, Switzerland) was used for all propagating SPR measurements reported here. The mannose-functionalized substrate was incorporated into BIAcore cassettes by gluing the chip into the cassettes using a Devcon two-part epoxy (Danvers, MA). Phosphate buffered saline (PBS), pH 7.4, was used as the running buffer and measurements were reported as changes in resonance angle ($\Delta\theta$), where $1^\circ = 10000$ refractive unit (RU).

### F. LSPR spectroscopy

LSPR extinction measurements were taken using an Ocean Optics (Dunedin, FL) SD2000 fiber optically coupled spectrometer. All spectra in this study were from macroscopic measurements obtained in transmission mode using unpolarized white light with a probe diameter of ~2 mm. A home-built flow cell was used to control the surrounding environment of the Ag nanoparticles and to introduce the analytes. A reflection probe (Ocean Optics) was used to measure LSPR from silver film over nanosphere substrates, which are opaque. The reflection probe consists of a tight bundle of 13 optical fibers (12 illumination fibers around a collection fiber) with a useable wavelength range of 400–900 nm. All reflectance spectra were collected against a mirrorlike Ag film over glass substrate as a reference.

### G. SERS apparatus

A battery-powered Raman spectrometer (model Inspector Raman, diode laser excitation wavelength $\lambda_{ex} =$ 785 nm) was purchased from DeltaNu (Laramie, WY).[20] A titanium-sapphire laser (CW Ti: Sa, model 3900, Spectra Physics, Mountain View, CA) pumped by a solid-state diode laser (model Millenia Vs, Spectra Physics) was used to generate $\lambda_{ex}$ 750 nm. The SERS measurement system consists of an interference filter (Coherent, Santa Clara, CA), a 1″ holographic edge filter (Physical Optics Corporation, Torrance, CA), a single-grating monochromator with the entrance slit set at 100 μm (model VM-505, Acton Research Corporation, Acton, MA), a liquid-$N_2$-cooled charge-coupled device (CCD) detector (model Spec-10:400B, Roper Scientific, Trenton, NJ), and a data-acquisition system (Photometrics, Tucson, AZ). The spectral positions of the CCD pixels were calibrated using emission lines of known wavelengths from a neon lamp. All the measurements were performed in ambient conditions.

## III. RESULT AND DISCUSSION

### A. Localized and propagating surface plasmon resonance sensors: A study using carbohydrate binding protein

This section describes comparative sensor studies conducted on the specific interactions between carbohydrates and proteins using both conventional propagating SPR and the newly developed LSPR sensors. The binding of Concanavalin A (ConA) to mannose-functionalized self-assembled monolayers (SAMs) is chosen to highlight the similarities and differences between the responses of the real-time angle shift SPR and wavelength shift LSPR biosensors. Comprehensive nonspecific binding studies are performed to ensure that the observed signal is due to specific binding of ConA to mannose-functionalized surface. Finally, the first multiplexed $2 \times 1$ LSPR sensor is also demonstrated on a Ag nanoparticles based LSPR sensor.

The potential of SPR biosensors was realized in early 1980s by Liedberg and coworkers who were able to sense antibodies by observing the change in the critical angle when the antibodies bound selectively to a Au film.[21] Furthermore, in late 1990s, nanoparticle-based LSPR sensors were reported to detect biological[5,22–24] and chemical entities.[11] Both SPR and LSPR sensors are sensitive to the local refractive index changes that occur when target analyte binds to the metal film or nanoparticles. Surface refractive index sensors have an inherent advantage over conventional biosensors in that they do not require a chromophoric group or other labels to transduce the binding event. Furthermore, they require very little ligand purification due to the specific ligand/receptor binding of these sensors. Also, these sensors provide real-time information on the course of binding and are applicable over a broad range of binding affinities. Additionally, LSPR sensing elements are inherently the size of a single nanoparticle, making the LSPR sensors potentially applicable for in situ detection in biological systems.[11] The sensing capability of LSPR sensors can also be tuned by changing the shape, size, and material composition of the nanoparticles.[17,25]

The LSPR sensor was prepared by immobilizing NSL-fabricated Ag nanoparticles with ~5% malemide terminated disulfide, which was then functionalized with mannose. The mannose-functionalized Ag nanosensor was rinsed with ethanol and placed in a flow cell. The LSPR measurement was conducted on the sensor, yielding a maximum extinction wavelength ($\lambda_{max}$) at 636.5 nm under nitrogen [Fig. 2(a)]. Then, 19.8 μM Con A was injected into the flow cell and the Ag nanosensor was incubated at room temperature for 20 min. The sample was thoroughly rinsed in the selected buffer solution, and the LSPR $\lambda_{max}$ of the Ag nanotriangles was measured to be 654.3 nm, resulting in a 17.8 nm red-shift. The LSPR response ($\Delta\lambda_{max}$) seen when ConA binds to the mannose-functionalized surface has been previously described using the following equation:

$$\Delta\lambda_{max} = m\theta(n_{ConA} - n_{environment})\exp(-2d_{SAM}/1_d)\left[1 - \exp(-2d_{ConA}/1_d)\right] \quad , \tag{1}$$

where $m$ is the refractive index sensitivity of the Ag nanosensor ($m = 191$ nm per refractive index unit for Ag

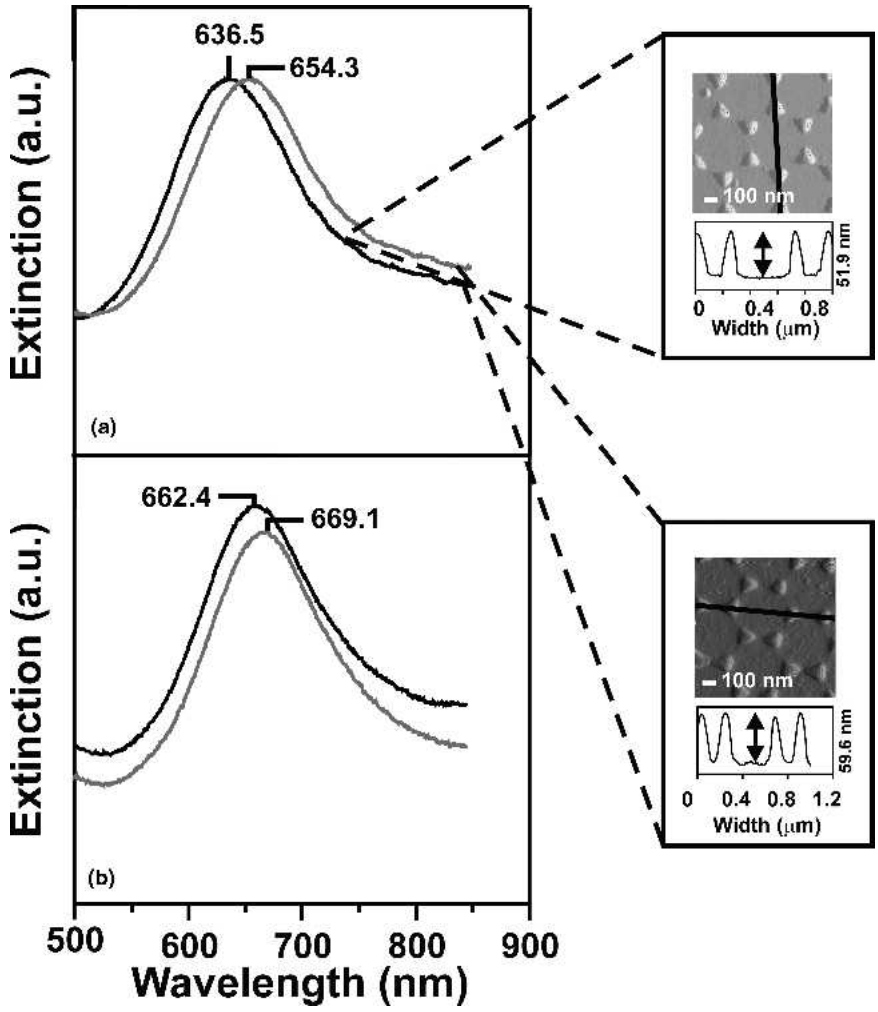


FIG. 2. (a) LSPR spectra of mannose-functionalized Ag nanosensor ($\lambda_{max}$ = 636.5 nm) and the specific binding of 19 μM ConA ($\lambda_{max}$ = 654.3 nm) in nitrogen. Inset shows tapping mode AFM image of the height increase when the Ag nanosensor is exposed to ConA (nanosphere diameter, $D$ = 390 nm; Ag thickness, $d_m$ = 50 nm; scan rate = 2 Hz; scan size 1 μm). (b) LSPR spectra of mannose-functionalized Ag nanobiosensor ($\lambda_{max}$ = 662.4 nm) and the specific binding of ConA to mannose ($\lambda_{max}$ = 669.1) in PBS buffer.

nanoparticles with in-plane-width of ~100 nm and out-of-plane height of 50 nm),[26] θ is the ConA surface coverage (for full surface coverage, θ = 1), $n_{ConA}$ is the refractive index of ConA, $n_{environment}$ is the refractive index of the environment in the cell ($n_{environment}$ = 1 for $N_2$, $n_{environment}$ = 1.33 for buffer, $n_{ConA}$ = 1.57),[27] $d_{SAM}$ is the thickness of EG3 layer ($d_{SAM}$ = 2 nm),[28] $d_{ConA}$ is the thickness of ConA layer, and $l_d$ is the characteristic of the Ag nanosensor ($l_d \approx$ 5–6 nm for Ag nanoparticles with in-plane-width of ~100 nm and out-of-plane height of 50 nm).[24]

Additionally, the LSPR response of ConA binding to the mannose-functionalized on Ag nanosensor was measured directly in a buffer environment resulting in a 6.7 nm red shift [Fig. 2(b)]. The 60% reduction of signal in buffer relative to $N_2$ environment is predicted by Eq. (1) and has been previously observed. The binding of ConA to mannose-functionalized surfaces was confirmed by height changes in atomic force microscope (AFM) measurements. After ConA incubation, the average nanoparticle height was increased by 7.7 nm. This result corresponds to the thickness of a monolayer of ConA as estimated from its x-ray structure.[29]

Furthermore, to compare the LSPR sensor with the well-established SPR sensor, the real-time response of the flat surface SPR sensor [Fig. 3(a)] and the LSPR Ag nanosensor [Fig. 3(b)], the SPR response (Δθ) and LSPR $\Delta\lambda_{max}$ response to the ConA binding on the mannose-functionalized surface was investigated. First, SPR Δθ response of the mannose-functionalized Au surface in a running buffer environment was recorded, followed by 19 μM ConA injection. Then the sensor was flushed with buffer for removal of nonspecifically bound ConA and a partial dissociation of ConA bound as the 1:1 mannose complex. Figure 3(a) illustrates the real-time monitoring of ConA by the SPR Δθ shift. Similarly, the real-time

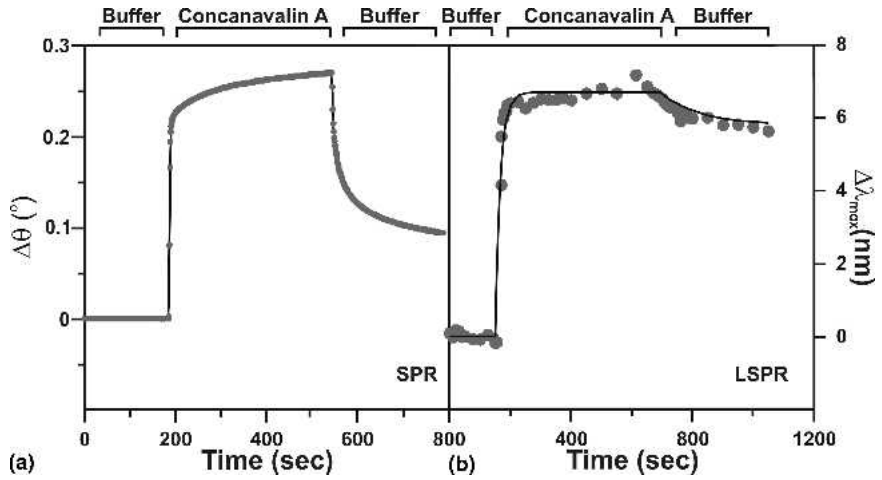


FIG. 3. Real-time response of sugar-functionalized sensor as 19 μM of ConA was injected in the cell following buffer injection: (a) mannose-functionalized SPR sensor and (b) mannose-functionalized Ag nanosensor. The points are the experimental data. The solid line for the SPR measurement is composed of straight line segments connecting the experimental data. The solid line in LSPR measurement is a first-order adsorption kinetics fit to the data and should only be interpreted as a guide to the eye.

LSPR response of ConA binding to the mannose-functionalized Ag nanonsensor was also probed [Fig. 3(b)].

Both the SPR and LSPR sensors showed a rapid response when ConA was exposed to the surface during the association phase, which indicates strong 1:1 mannose/ConA binding on the surface[30] followed by weak non-specific binding. However during the dissociation phase, the response of the SPR sensor decreased by 60% whereas the response of the LSPR sensor decreased only by 14%. Our hypothesis to explain this difference is the long range decay length of the SPR sensor electromagnetic field ($l_d \approx 200$ nm),[27] compared to that of the LSPR sensor ($l_d \approx 5$ to 6 nm). The dissociation response seen in the SPR sensor is caused by removal of non-specifically bound ConA, partial dissociation of 1:1 bound ConA with mannose, and change in bulk refractive index from ConA/buffer to only buffer. However, due to shorter decay length of the electromagnetic field of the LSPR sensor, the dissociation response seen can be attributed to only removal of nonspecifically bound ConA and partial dissociation of bound ConA.

LSPR sensors should have no nonspecific bindings to other proteins to be a viable sensor. Two non-specific binding studies listed below were performed to verify that the LSPR responses seen when ConA binds to the mannose functionalized surface is due solely to specific binding between the ligand and the receptor.

### 1. Erythrina crystagalli interacting with the mannose functionalized sensor

Erythrina crystagalli (Ery) is a dimer plant lectin with the molecular weight of 56 kDa that specifically binds to galactose.[31] The Ag nanosensors were exposed to Ery to demonstrate that the mannose-functionalized Ag nanosensors do not have an affinity toward lectins other than mannose binding lectins. The Ag nanosensors functionalized with mannose SAMs had a LSPR $\lambda_{max}$ of 677.5 nm [Fig. 4(a)]. Incubation of the sensor in 26 μM Ery resulted in a LSPR $\lambda_{max}$ of 677.7 nm. The 0.2 nm shift corresponds to the instrumental noise wavelength shift in the baseline, illustrating that lectins not specific to mannose do not bind to the mannose-functionalized sensor surface.

### 2. Bovine serum albumin interacting with the mannose-functionalized sensor

The Ag nanosensors were exposed to a bovine serum albumin (BSA) solution to demonstrate that these LSPR sensors do have nonspecific interaction with other proteins. The Ag nanoparticles were functionalized with mannose thiols giving a LSPR $\lambda_{max}$ of 645.6 nm [Fig. 4(b)]. Incubation of the sensor in 29 μM BSA resulted in a LSPR $\lambda_{max}$ of 645.5 nm, which is also equal to the instrumental noise.

In this study, we tested the first step toward fabricating a multiplexed LSPR sensor, which enjoys several advantages such as rapid and parallel detection, low volume of analytes, and low cost. Herein, we demonstrate a primitive 2 × 1 multiplexed LSPR sensor. A (2 × 1) LSPR carbohydrate sensing chip sensor consists of a glass substrate with nanoparticle arrays of two different heights (namely, 35 and 75 nm). The 35 nm nanoparticle arrays were functionalized with galactose resulting into a LSPR $\lambda_{max}$ of 724.5. Similarly, 75 nm nanoparticle arrays were functionalized with mannose resulting into a LSPR $\lambda_{max}$ of 677.7 nm. To prevent the mixing of the sugar thiol solutions, the nanoparticle array elements were separated by a poly(dimethyl siloxane) separator and removed

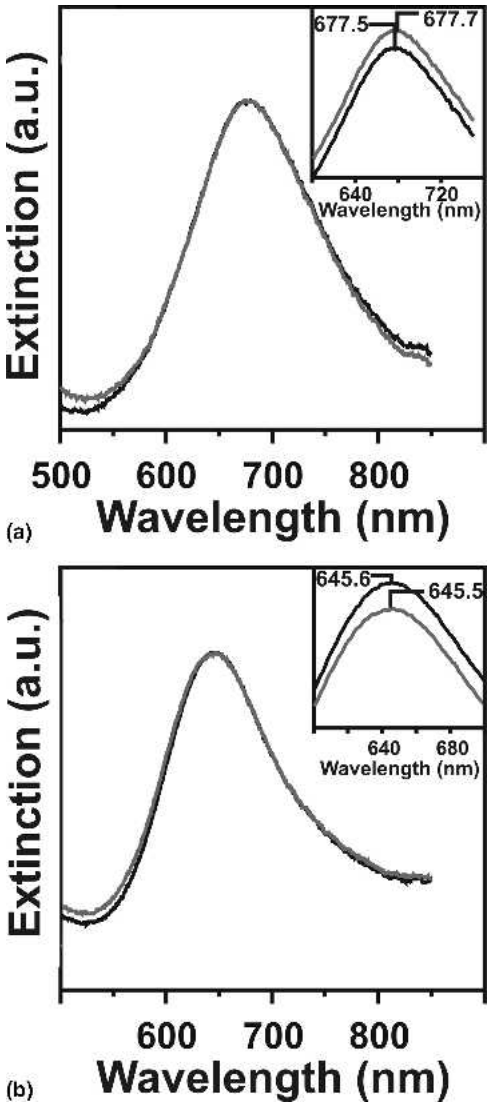


FIG. 4. Nonspecific binding study on mannose-functionalized Ag nanosensor with two different proteins. All extinction measurements were taken in PBS buffer. All insets magnify the extinction spectra, and the İmax are denoted. (a) LSPR spectra illustrating nonspecific binding of Ery (26 μM) to the mannose-functionalized surface. (b) LSPR spectra illustrating nonspecific binding of bovine serum albumin (29 μM) to the mannose-functionalized surface.

before exposing the surface to ConA. The galactose and mannose-functionalized carbohydrate sensing chip was exposed to 19 μM ConA and rinsed with PBS buffer resulting in a LSPR $\lambda_{max}$ of 724.6 nm and 682.7 nm (Fig. 5).

When ConA binds to the mannose-functionalized surface, a 5-nm shift is seen, and when the ConA binds to the galactose-functionalized surface, a 0.1-nm shift is observed, indicating that no binding occurs. The decrease in the LSPR shift seen when ConA binds to the mannose-functionalized Ag nanosensor with out-of-plane height of 75 nm is attributed to the lower refractive index sensitivity of taller nanoparticles.

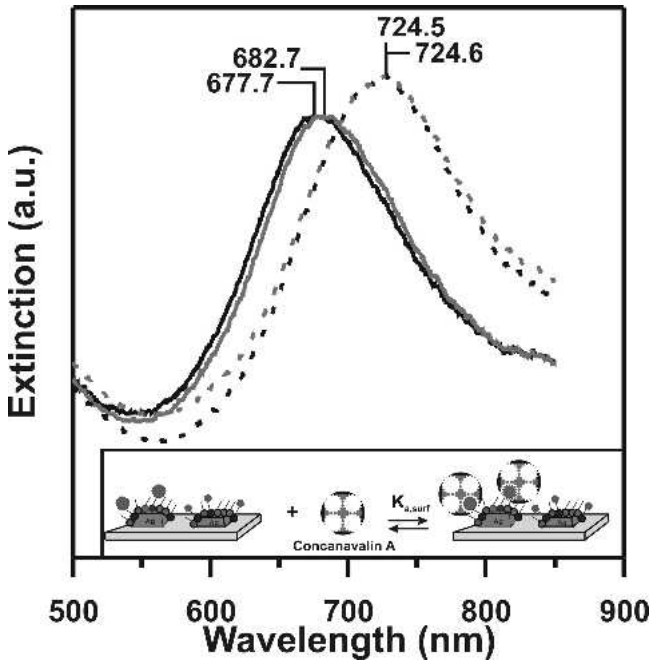


FIG. 5. LSPR spectra illustrating multiplexing Ag nanosensor carbochip. Inset shows the schematic of selective ConA binding to the mannose-functionalized portion of the chip. Reproduced with permission from Ref. 5, © 2004 American Chemical Society.

### B. Optimized silver film over nanosphere surfaces for the biowarfare agent detection based on surface-enhanced raman spectroscopy

Vibrational spectroscopic methods are valuable analytical tools because they yield not only quantitative information but also unique vibrational signatures for small molecule analytes. Raman spectroscopy, in all its forms, is a vibrational spectroscopic method that has the inherent ability to distinguish between molecules with great similarity. High laser powers and long acquisition times are usually required to achieve high-quality Raman spectra due to the inherently small normal Raman scattering cross section of many molecules of interest. In contrast, higher intensity Raman signals and lower detection limits can be achieved using SERS. SERS produces very large enhancements in the effective Raman cross section of species spatially confined within the zone of the electromagnetic fields (namely, 0–4 nm) generated upon excitation of the LSPR of nanostructured noble metal surfaces.[14] The Raman signals of ensemble-averaged molecules show enhancement of up to 8 orders of magnitude,[32,33] while the signals from single molecules can show an increase by 14 to 15 orders of magnitude in special cases.[34,35] In comparison with infrared and normal Raman spectroscopies, SERS enjoys the advantages of application in aqueous media and the sensitivity sufficient for trace level detection.

Previous studies have demonstrated that the substrates with a highly tunable LSPR are readily used to maximize

SERS intensities, which accordingly lowers analytical limit of detection (LOD).[32,33] Early SERS substrates contained a random distribution of roughness feature sizes produced by oxidation-reduction cycling on a metal electrode or evaporation of a thin metal film onto a flat substrate.[36] In recent years, researchers have explored the optimal size, shape, spacing, and pattern of noble metal nanoparticles on surfaces to optimize SERS enhancements.[32,33] One of the most robust SERS substrates in use today is the metal film over nanospheres substrates prepared by NSL (Fig. 1). The diameter of the nanospheres ($D$) and the thickness of the metal film ($d_m$) determine the size distribution of the roughness features and, hence, the optical response. The uniform polystyeren sphere templates confine the pattern and geometry of AgFON substrates that usually generate a LSPR with a full width at half-maximum of ~200 nm. Recent experiments have conclusively demonstrated that MFON substrates are stable for months and remain SERS-active even when exposed to large temperature[37] and potential excursions.[38] The utility of the MFON substrate is demonstrated herein as a robust SERS substrate used in the rapid detection of *Bacillus subtilis* spores, harmless simulants for *Bacillus anthracis*. A bacillus spore structurally consists of several protective layers and a core cell. Calcium dipicolinate (CaDPA) exists in these protective layers and can be used as the spore biomarker because other potentially interfering species lack this particular molecule in such high proportions.[39]

AgFON substrates for SERS measurements using 750-nm laser excitation were optimized by first measuring the dependence of the LSPR spectral position on nanosphere diameter. The LSPR measurements were conducted on the AgFON substrates with nanospheres having diameters of 390, 510, 600, and 720 nm. In Fig. 6 the reflectance spectrum of AgFON substrate, with $D = 600$ nm and $d_m = 200$ nm, shows a reflectivity minimum near 753 nm. This substrate is expected to show the largest intensity for 750 nm laser excitation.

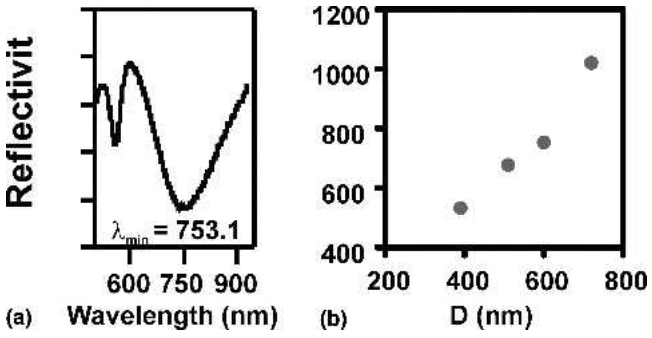


FIG. 6. (a) The reflectance spectra of a AgFON substrate ($D = 600$ nm, $d_m = 200$ nm) demonstrated a LSPR $\lambda_{min}$ at ~753 nm. (b) LSPR versus nanosphere diameter. The AgFON substrates were made from sphere masks using 390-, 510-, 600-, and 720-nm-diameter spheres. For all the spectra, $d_m = 200$ nm.

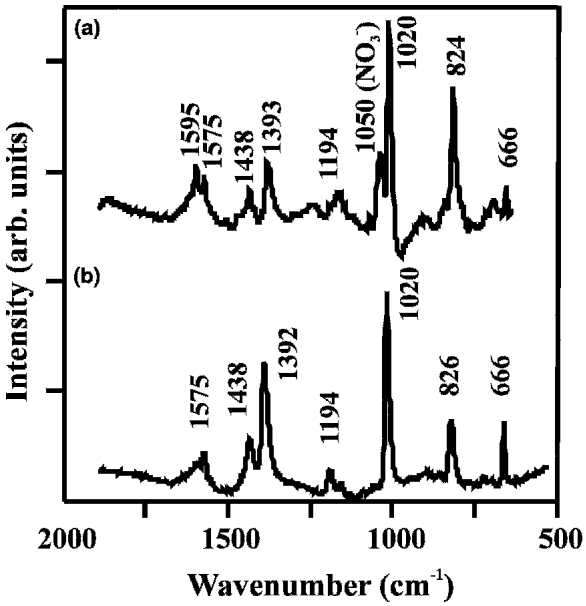


FIG. 7. (a) SERS spectrum of $3.1 \times 10^{-13}$ M spore suspension on a AgFON substrate. (b) SERS spectrum of $5.0 \times 10^{-4}$ M CaDPA. $\lambda_{ex} = 750$ nm, laser excitation power $P_{ex} = 50$ mW, acquisition time = 1 min.

Further confirmation, by comparing benzenethiol Raman signals from theses substrates, has been shown in our previous work.[8]

CaDPA was extracted from spores by sonicating a spore suspension in 0.02 M $HNO_3$ solution for 10 min. A $3.1 \times 10^{-13}$ M spore suspension ($3.7 \times 10^4$ spores in 0.2 μl, 0.02 M $HNO_3$) was deposited onto a AgFON substrate for the SERS measurement. In comparison, parallel SERS measurements of CaDPA were performed. High signal-to-noise ratio (S/N) SERS spectrum was obtained in a 1-min data acquisition period [Fig. 7(a)]. Clearly, the spectrum of spores is dominated by bands associated with CaDPA [Fig. 7(b)]. The peak at 1050 $cm^{-1}$ in Fig. 7 is from the symmetrical stretching vibration of $NO_3^-$,[8] which was selected as the internal standard to reduce the sample to sample deviations.

The SERS signal from extracted CaDPA was measured over the spore concentration range $10^{-14}$ to $10^{-12}$ M to determine the saturation binding capacity of the AgFON surface. In Fig. 8(a), each data point represents the average intensity at 1020 $cm^{-1}$ (a ring breathing mode) from three samples with the standard deviation shown by the error bars. The binding curve provides three important characteristics that describe the binding of extracted CaDPA to a AgFON substrate. First, at low spore concentrations, the peak intensity increases linearly with concentration [Fig. 8(a), inset]. The LOD for *B. subtilis* spores was found to be $2.1 \times 10^{-14}$ M ($2.6 \times 10^3$ spores in 0.2 μl, 0.02 M $HNO_3$), as calculated by extrapolation of the linear concentration range of the adsorption isotherms. In this case, the LOD is defined as the

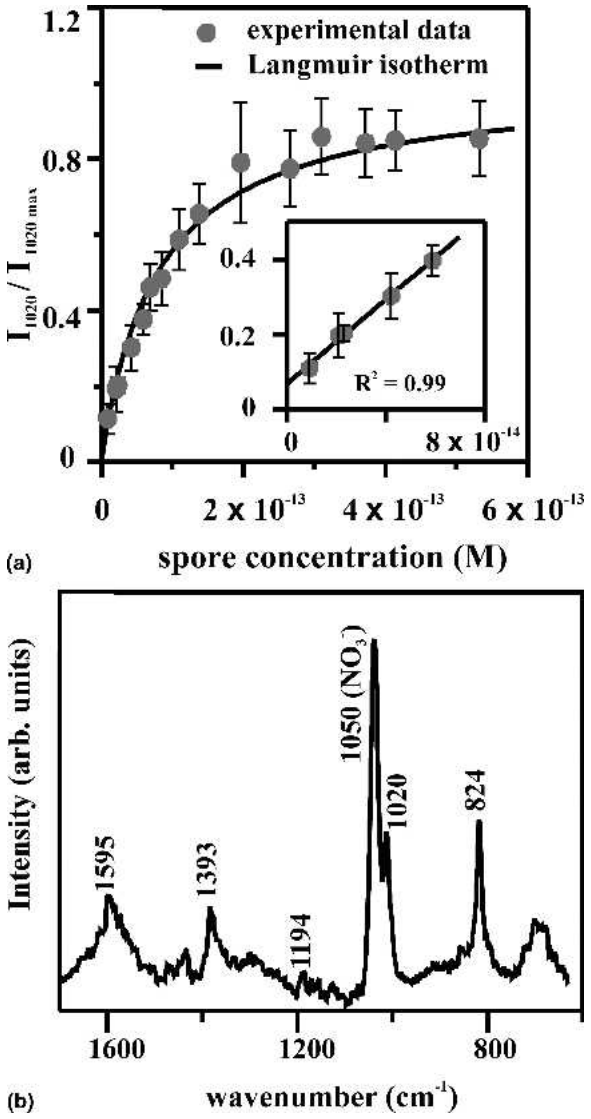


FIG. 8. (a) Adsorption isotherm for *B. subtilis* spore suspension onto a AgFON substrate. $I_{1020}$ was taken from SERS spectra that correspond to varying spore concentrations in 0.2 μl, 0.02 M $HNO_3$ on AgFON substrates. $\lambda_{ex}$ = 750 nm, $P_{ex}$ = 50 mW, acquisition time = 1 min, $D$ = 600 nm, and $d_m$ = 200 nm. The inset shows the linear range that is used to determine the LOD. Each data point represents the average value from three SERS spectra. Error bars show the standard deviations. (b) SERS spectrum of $2.1 \times 10^{-14}$ M spore suspension ($2.6 \times 10^3$ spores in 0.2 μl, 0.02 M $HNO_3$) on AgFON. $\lambda_{ex}$ = 750 nm, $P_{ex}$ = 50 mW, acquisition time = 1 min. Reproduced with permission from Ref. 8, © 2005 American Chemical Society.

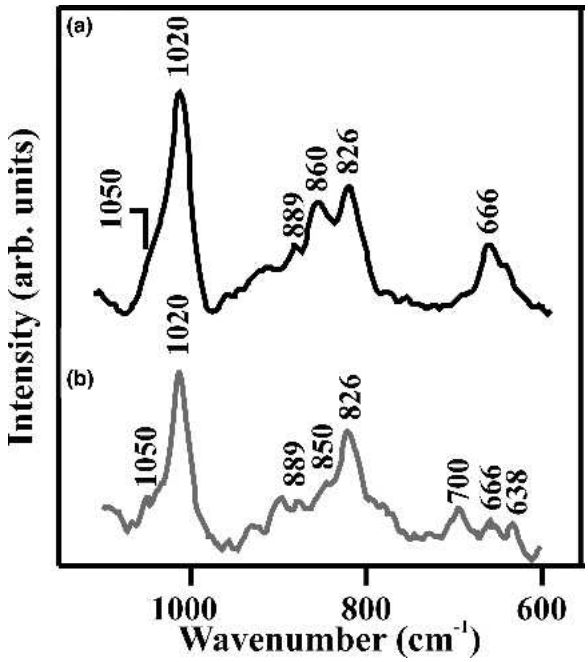


FIG. 9. SERS spectra obtained by portable Raman spectrometer: (a) SERS spectrum of $8.3 \times 10^{-14}$ M spore suspension ($1.0 \times 10^4$ spores in 0.2 μl, 0.02 M $HNO_3$) on 30-day old AgFON and (b) SERS spectrum of $10^{-4}$. M CaDPA in 0.2 μL 0.02 M $HNO_3$ on 30-day-old AgFON substrate. $\lambda_{ex}$ = 785 nm, $P_{ex}$ = 35 mW, acquisition time = 5 s, resolution = 15 $cm^{-1}$, $D$ = 600 nm, and $d_m$ = 200 nm. Reproduced with permission from Ref. 8, © 2005 American Chemical Society.

concentration of spores for which the strongest SERS signal of CaDPA at 1020 $cm^{-1}$ is equal to three times the background SERS signal within a 1-min acquisition period. Furthermore, a similar spore concentration $2.1 \times 10^{-14}$ M was used to test the LOD prediction. A 1-min acquisition yields a SERS spectrum that clearly demonstrates the spore Raman features [Fig. 8(b)] in comparison with Fig. 7(a). These data demonstrate that the SERS LOD is well below the anthrax infectious dose of $10^4$ spores. The second important characteristic determined by the binding curve is the saturation response can be determined to be ~$2 \times 10^{-13}$. Finally, the response curve yielded a surface binding constant $1.7 \times 10^{13}$ $m^{-1}$.[8]

As a first step toward developing a rapid and portable anthrax detection protocol, the Raman spectrum from $10^4$ *B. subtilis* spores dosed onto a 1-month-old AgFON substrate was readily acquired using a commercially available portable Raman instrument. A high S/N spectrum was achieved within five seconds [Fig. 9(a)]. The SERS peak positions and intensity pattern for the spore sample was similar to those of CaDPA recorded utilizing the same device [Fig. 9(b)]. This is the first example of using a compact, portable Raman spectrometer for the detection of bacillus spores.

## IV. CONCLUSION

In this work, we have summarized our representative accomplishments in sensing applications using localized surface plasmon resonance and surface-enhanced Raman spectroscopy. We compared the responses of a SPR sensor with a LSPR sensor using the binding of ConA to a mannose-functionalized SAM surface. Real-time angle shift SPR and wavelength shift LSPR measurements

exhibited comparable magnitude saturation coverage responses during the association phase when ConA specifically bound to mannose ligand. However, during the dissociation phase, the signal loss for SPR sensor was 5 times greater than that of the LSPR sensor. In addition, to verify that the response seen on the LSPR sensor was due to the specific binding of ConA to the mannose-functionalized Ag nanosensor, several nonspecific binding studies were performed. Finally, this work demonstrates the first multiplexed version of a LSPR carbohydrate sensing chip to study the affinity of ConA on the mannose and galactose-functionalized surface.

We also presented the rapid detection of *Bacillus subtilis* spores using surface-enhanced Raman spectroscopy on silver film over nanosphere substrates. The calcium dipicolinate biomarker can be extracted effectively from spores with nitric acid and successfully detected by SERS. The highly tunable nature of AgFON optical properties was exploited to establish general optimization conditions. AgFON surfaces optimized for 750-nm laser excitation have been characterized by LSPR reflectance spectroscopy. The SERS signal from extracted CaDPA was evaluated over the spore concentration range $10^{-15}$ to $10^{-12}$ M to determine the adsorption capacity of the AgFON surface and the limit of detection. These sensing capabilities have been successfully transitioned to an inexpensive, portable Raman spectrometer. Using the extraction method and this field-portable instrument, the anthrax infectious dose of $10^4$ spores were detected with only a 5-s collection period on a 1-month-old prefabricated AgFON substrate.

## ACKNOWLEDGMENT

The authors gratefully acknowledge Ms. Liza Babayan, Dr. Haitao Ji, and Dr. Douglas A. Stuart for their technical assistance and helpful discussions. This work was supported by the Nanoscale Science and Engineering Initiative of the National Science Foundation under NSF Award EEC-0118025, the National Science Foundation (DMR-0076097), the Air Force Office of Scientific Research Multidisciplinary University Research Initiative (MURI) program (F49620-02-1-0381), and a Northwestern University Materials Research Science and Engineering Center (MRSEC) Fellowship (X. Zhang). Any opinions, findings, and conclusions or recommendations expressed in this paper are those of the authors and do not necessarily reflect those of the National Science Foundation.

## REFERENCES

1. J. Ji, J.A. Schanzle, and M.B. Tabacco: Real-time detection of bacterial contamination in dynamic aqueous environments using optical sensors. *Anal. Chem.* **1411,** 76 (2004).
2. F.S. Ligler, C.R. Taitt, L.C. Shriver-Lake, K.E. Sapsford, Y. Shubin, and J.P. Golden: Array biosensor for detection of toxins. *Anal. Bioanal. Chem.* **469,** 377 (2003).
3. C.R. Yonzon, C.L. Haynes, X. Zhang, J.T. Walsh, and R.P. Van Duyne: A glucose biosensor based on surface-enhanced raman scattering: Improved partition layer, temporal stability, reversibility, and resistance to serum protein interference. *Anal. Chem.* **78,** 76 (2004).
4. D.A. Stuart, C.R. Yonzon, X. Zhang, O. Lyandres, N.C. Shah, M.R. Glucksberg, J.T. Walsh, and R.P. Van Duyne: Glucose sensing using near infrared surface-enhanced raman spectroscopy: Gold surfaces, 10-day stability, and improved accuracy. *Anal. Chem.* **4013,** 77 (2005).
5. C.R. Yonzon, E. Jeoung, S. Zou, G.C. Schatz, M. Mrksich, and R.P. Van Duyne: A comparative analysis of localized and propagating surface plasmon resonance sensors: The binding of concanavalin A to a monosaccharide functionalized self-assembled monolayer. *J. Am. Chem. Soc.* **12669,** 126 (2004).
6. H. Ho and M. Leclerc: Optical sensors based on hybrid aptamer/conjugated polymer complexes. *J. Am. Chem. Soc.* **1384,** 126 (2004).
7. S.L. Wiskur and E.V. Anslyn: Using a synthetic receptor to create an optical-sensing ensemble for a class of analytes: A colorimetric assay for the aging of scotch. *J. Am. Chem. Soc.* **10109,** 123 (2001).
8. X. Zhang, M.A. Young, O. Lyandres, and R.P. Van Duyne: Rapid detection of an anthrax biomarker by surface-enhanced raman spectroscopy. *J. Am. Chem. Soc.* **4484,** 127 (2005).
9. H. Reather: *Surface Polaritons on Smooth and Rough Surfaces and on Gratings* (Springer-Verlag, Berlin, Germany, 1988).
10. T.R. Jensen, G.C. Schatz, and R.P. Van Duyne: Nanosphere lithography: Surface plasmon resonance spectrum of a periodic array of silver nanoparticles by UV-vis extinction spectroscopy and electrodynamic modeling. *J. Phys. Chem. B* **2394,** 103 (1999).
11. A.D. McFarland and R.P. Van Duyne: Single silver nanoparticles as real-time optical sensors with zeptomole sensitivity. *Nano Lett.* **1057,** 3 (2003).
12. T.R. Jensen, M.D. Malinsky, C.L. Haynes, and R.P. Van Duyne: Nanosphere lithography: Tunable localized surface plasmon resonance spectra of silver nanoparticles. *J. Phys. Chem. B* **10549,** 104 (2000).
13. J. Yguerabide and E.E. Yguerabide: Light-scattering submicroscopic particles as highly fluorescent analogs and their use as tracer labels in clinical and biological applications—II. Experimental characterization. *Anal. Biochem.* **157,** 262 (1998).
14. G.C. Schatz and R.P. Van Duyne: Electromagnetic mechanism of surface-enhanced spectroscopy, in *Handbook of Vibrational Spectroscopy,* edited by J.M. Chalmers and P.R. Griffiths (Wiley, New York, 2002), pp. 759–774.
15. C. Siemes, A. Bruckbauer, A. Goussev, A. Otto, M. Sinther, and A. Pucci: SERS-active sites on various copper substrates. *J Raman Spectrosc.* **231,** 32 (2001).
16. M. Graff, J. Bukowska, and K. Zawada: Surface enhanced raman scattering (SERS) of 1-hydroxybenzotriazole adsorbed on a copper electrode surface. *J. Electroanal. Chem.* **297,** 567 (2004).
17. C.L. Haynes and R.P. Van Duyne: Nanosphere lithography: A versatile nanofabrication tool for studies of size-dependent nanoparticle optics. *J. Phys. Chem. B* **5599,** 105 (2001).
18. B.T. Houseman, E.S. Gawalt, and M. Mrksich: Maleimide-functionalized self-assembled monolayers for the preparation of peptide and carbohydrate biochips. *Langmuir* **1522,** 19 (2003).
19. G.F. Bailey, S. Karp, and L.E. Sacks: Ultraviolet-absorption spectra of dry bacterial spores. *J. Bacteriol.* **984,** 89 (1965).
20. Deltanu company home page, www.deltanu.com (2005).
21. B. Liedberg, C. Nylander, and I. Lundstorm: Surface plasmon

resonance for gas detection and biosensing. *Sens. Actuators B* **229,** 4 (1983).
22. G. Raschke, S. Kowarik, T. Franzl, C. Sönnichsen, T.A. Klar, J. Feldmann, A. Nichtl, and K. Kürzinger: Biomolecular recognition based on single gold nanoparticle light scattering. *Nano Lett.* **935,** 3 (2003).
23. J.C. Riboh, A.J. Haes, A.D. McFarland, C.R. Yonzon, and R.P. Van Duyne: A nanoscale optical biosensor: Real-time immunoassay in physiological buffer enabled by improved nanoparticle adhesion. *J. Phys. Chem. B* **1772,** 107 (2003).
24. A.J. Haes and R.P. Van Duyne: A nanoscale optical biosensor: Sensitivity and selectivity of an approach based on the localized surface plasmon resonance spectroscopy of triangular silver nanoparticles. *J. Am. Chem. Soc.* **10596,** 124 (2002).
25. A.J. Haes, S. Zou, G.C. Schatz, and R.P. Van Duyne: A nanoscale optical biosensor: The long range distance dependence of the localized surface plasmon resonance of noble metal nanoparticles. *J. Phys. Chem. B* **109,** 108 (2004).
26. M.D. Malinsky, K.L. Kelly, G.C. Schatz, and R.P. Van Duyne: Chain-length dependence and sensing capabilities of the localized surface plasmon resonance of silver nanoparticles chemically modified with alkanethiol self-assembled monolayers. *J. Am. Chem. Soc.* **1471,** 123 (2001).
27. L.S. Jung, C.T. Campbell, T.M. Chinowsky, M.N. Mar, and S.S. Yee: Quantitative interpretaion of the response of surface plasmon resonance sensors to adsorbed films. *Langmuir* **5636,** 14 (1998).
28. C. Palegrosdemange, E.S. Simon, K.L. Prime, and G.M. Whitesides: Formation of self-assembled monolayers by chemisorption of derivatives of oligo(ethylene glycol) of structure HS(CH2)11(Och2CH2) meta-OH on gold. *J. Am. Chem. Soc.* **12,** 113 (1991).
29. K.D. Hardman and C.F. Ainsworth: Structure of Concanavalin A at 2.4-ang resolution. *Biochemistry* **4910,** 11 (1972).
30. E.A. Smith and R.M. Corn: Surface plasmon resonance imaging as a tool to monitor biomolecular interaction in an array based format. *Appl. Spectrosc.* **320A,** 57 (2003).
31. D. Gupta, M. Cho, R.D. Cummings, and C.F. Brewer: Thermodynamics of carbohydrate binding to galectin-1 from Chinese hamster ovary cells and two mutants. A comparison with four galactose-specific plant lectins. *Biochemistry.* **15236,** 35 (1996).
32. A.D. McFarland, M.A. Young, J.A. Dieringer, and R.P. Van Duyne: Wavelength-scanned surface-enhanced raman excitation spectroscopy. *J. Phys. Chem. B* **109,** 11279 (2005).
33. C.L. Haynes and R.P. Van Duyne: Plasmon-sampled surface-enhanced Raman excitation spectroscopy. *J. Phys. Chem. B* **7426,** 107 (2003).
34. S. Nie and S.R. Emory: Probing single molecules and single nanoparticles by surface-enhanced Raman scattering. *Science* **1102,** 275 (1997).
35. K. Kneipp, Y. Wang, H. Kneipp, L.T. Perelman, I. Itzkan, R.R. Dasari, and M.S. Feld: Single molecule detection using surface-enhanced Raman scattering (SERS). *Phys. Rev. Lett.* **1667,** 78 (1997).
36. A.M. Stacy and R.P. Van Duyne: Surface enhanced Raman and resonance Raman-spectroscopy in a non-aqueous electrochemical environment—tris(2,2′-bipyridine)ruthenium(II) adsorbed on silver from acetonitrile. *Chem. Phys. Lett.* **365,** 102 (1983).
37. M. Litorja, C.L. Haynes, A.J. Haes, T.R. Jensen, and R.P. Van Duyne: Surface-enhanced Raman scattering detected temperature programmed desorption: Optical properties, nanostructure, and stability of silver films over $SiO_2$ nanospheres. *J. Phys. Chem. B* **6907,** 105 (2001).
38. X. Zhang, C.R. Yonzon, and R.P. Van Duyne: An electrochemical surface-enhanced raman spectroscopy approach to anthrax detection. *Proc. SPIE* **82,** 5221 (2003).
39. R. Goodacre, B. Shann, R.J. Gilbert, E.M. Timmins, A.C. McGovern, B.K. Alsberg, D.B. Kell, and N.A. Logan: Detection of the dipicolinic acid biomarker in bacillus spores using curie-point pyrolysis mass spectrometry and fourier transform infrared spectroscopy. *Anal. Chem.* **119,** 72 (2000).